Characterization of Tetrahedral Vanadium-Containing MCM-41 Molecular Sieves Synthesized at Room Temperature

M. Chatterjee,* T. Iwasaki, H. Hayashi, Y. Onodera, T. Ebina, and T. Nagase

Inorganic Materials Section, Tohoku National Industrial Research Institute, 4-2-1 Nigatake, Miyagino-ku, Sendai 983-8551, Japan

Received December 29, 1998. Revised Manuscript Received February 8, 1999

A series of mesoporous vanadosilicate V−MCM-41 molecular sieves with variable Si/V ratios have been synthesized at room temperature using a minimum amount of template. The chemical environment of the vanadium centers in V−MCM-41 was investigated by powder X-ray diffraction (XRD), transmission electron microscopy (TEM), Fourier transform infrared (FTIR) spectroscopy, diffuse reflectance UV−visible (UV−vis) spectroscopy, electron spin resonance (ESR), and ^{29}Si and ^{51}V nuclear magnetic resonance (NMR), and the optimal synthesis condition have been established. The increase of the unit cell parameter and decrease of Q_3/Q_4 ratio of ^{29}Si NMR spectra with vanadium content suggest the incorporation of vanadium in the framework of the MCM-41 structure. UV−vis and ^{51}V NMR studies confirm the presence of V^{5+} ion in the tetrahedral position. In the case of a freshly synthesized sample, VO^{2+} in a square pyramidal arrangement was detected by ESR. After calcination, V^{5+} species remain in the tetrahedral arrangement, confirming the stability of the material. Moreover, these solids were found to be catalytically active in the oxidation of toluene and hydroxylation of benzene with H_2O_2.

Introduction

The use of titanium- and vanadium-modified molecular sieves of different structure types that act as catalysts in liquid-phase oxidation with H_2O_2 as the oxidant has been well-documented.[1,2] The activity and the selectivity of these catalysts were found to be sensitive to the nature of vanadium species in the matrix, which includes the oxidation state, coordination state, dispersion, and stability.[1,3−5] Besides these (oxidation state, coordination state, dispersion) structural features of macroporous and microporus support also have noticeable effects on the form of vanadium species and its catalytic behavior. However, most of the vanadium-modified molecular sieves were microporous solids with channels less than 10 Å that restrict the oxidation of large organic molecules. In 1992 Beck and co-workers [6,7] described a new family of mesoporous silicate designated as M41S. The properties of this material with pore diameter and chemical composition can be varied over a broad range. Hence, several research groups have attempted to incorporate vanadium into the hexagonal tubular silica material MCM-41. MCM-41 possesses uniform mesopore channels varying from 15 to 100 Å. Abe et al.[8] and Luca et al.[9] synthesized nonsilica-based hexagonal mesoporous material. Despite these achievements, the vanadium centers in these materials were unstable. So far, the direct hydrothermal synthesis of vanadium-substituted MCM-41 was first achieved by Reddy et al.[10] The sample obtained by that method after 6 days of heat treatment contained dispersed vanadium centers. Gontier et al.[4] observed that vanadium cations in synthetic V−MCM-41 were probably in a coordination state like those in aqueous solution. Morey et al.[11] prepared the mesoporous material V−MCM-48 using an impregnation method. ByUV−visible spectrscopy (UV−vis) measurement they suggested that the hydroxyl group on the wall of the MCM-48 were employed as anchoring sites of vanadium ions to form pseudooctahedral $O_{3/2}V{=}O$ graft on the mesoporous wall. A spectroscopic characterization of vanadium-containing MCM-41 obtained by the hydrothermal method describing two different sites of anchoring for vanadium was presented by Zhaohua Luan et al.[12]

* Corresponding author. E-mail: maya@tniri.go.jp. Telephone: 81-22-237-5211. Fax: 81-22-236-6839.

(1) Whittington, B. I.; Anderson, J. R. *J. Phys. Chem.* **1991**, *95*, 3306.
(2) Taramasso, M.; Perego, G.; Notari, B. U.S. Patent 4,410501, 1983.
(3) (a) Oyama, S. T.; Went, G. T.; Lewis, K. B.; Bell, A. T.; Somarjai, G. A. *J. Phys. Chem.* **1989**, *93*, 6786. (b) Went, G. T.; Oyama, S. T.; Bell, A. T. *J. Phys. Chem.* **1990**, *94*, 4240.
(4) Gontier, S.; Tuel, A. *Microporous Mater.* **1995**, *5*, 161.
(5) Morey, M.; Davidson, A.; Eckert, H.; Stucky, G. *Chem. Mater.* **1996**, *8*, 486.
(6) Kresege, C. T.; Leonowicz, M. E.; Roth, W. J.; Vartuli, J. C.; Beck, J. S. *Nature* **1992**, *359*, 710.
(7) Beck, J. S.; Vartuli, J. C.; Roth, W. J.; Leonowicz, M. E.; Kresege, C. T.; Schmitt, K. D.; Chu, C. T.−W.; Olsen, D. H.; Sheppard, E. W.; McCullen, S. C.; Higgins, J. B.; Schlenker, J. L. *J. Am. Chem. Soc.* **1992**, *114*, 10834.
(8) Abe, T.; Taguchi, A.; Iwamoto, M. *Chem. Mater.* **1995**, *7*, 1429.
(9) Luca, V.; Maclachlan, D. J.; Hook, J. M.; Withers, R. *Chem. Mater.* **1995**, *7*, 2220.
(10) Reddy, K. M.; Moudrakovski, I.; Sayari, A.; *J. Chem. Soc., Chem. Commun.* **1994**, 1059.
(11) Morey, M.; Davidson, M.; Eckert, H.; Stucky, G. *Chem. Mater.* **1996**, *8*, 486.
(12) Luanm Z.; Xu, J.; He, H.; Klinowski, J.; Kevan, L. *J. Phys. Chem.* **1996**, *100*, 19595.

10.1021/cm981152k CCC: $18.00
Published on Web 04/24/1999

The framework of mesoporous M41S differs from that of microporous zeolite of three-dimensional tetrahedral networks and was constructed from amorphous silica around the rodlike miceller template of a cationic surfactant. ^{29}Si magic angle spinning nuclear magnetic resonance (MAS NMR) of M41S indicate the presence of an Si−OH group similar to defect sites in a zeolite that can act as anchors for the attachment of transition-metal species via intermolecular condensation. In the conventional method, transition-metal-substituted molecular sieves were generally obtained by using some phase stabilizer, such as 2-propanol (ref 12) and tetramethylammonium hydroxide (TMAOH). In this work our major goal is to develop a very simple process without using any phase stabilizer and TMAOH. Transition-metal-substituted molecular sieves effectively oxidize a variety of organic compounds with economical oxygen donors such as 30% aqueous hydrogen peroxide. The spectroscopic characterization of the catalyst using different techniques (e.g., XRD (X-ray diffraction), FTIR (Fourier transform infrared) spectroscopy, ESR (electron spin resonance), UV−vis spectroscopy, NMR) was carried out in order to give some insight to the location and state of vanadium in V−MCM-41. The presence of tetrahedral V^{5+} ions was necessary to carry out reversible redox cycles.

Experimental Section

Synthesis. The starting reaction mixture had a molar composition of 1/0.12:92.6 M/TEOS (tetraethyl orthosilicate): $(C_{16}H_{33}N(CH_3)_3$ Br); H_2O. Vanadyl sulfate solution was added according to the following ratios, Si/V = 20−200. The synthesized mixture was prepared using tetraethyl orthosilicate (NacalaiTasque, Japan), vanadyl sulfate trihydrate (Wako pure chemicals), cetyl trimethyl ammonium bromide (Merck), sodium hydroxide, and deionized water.

The synthesis procedure was as follows: 1.12 g of cetyl trimethyl ammonium bromide (CTAB) was added to 30 g of deionized water and stirred until a clear solution was obtained. Then, a 10 mL solution of vanadyl sulfate in water was added to the surfactant solution under stirring conditions. The addition of vanadyl sulfate solution was very slow and the mixture was stirred for 1 h. Then, 5.0 g of tetraethyl orthosilicate (TEOS) was added slowly under stirring conditions. Finally, the mixture was stirred for another 1 h. The pH of the resulting mixture was adjusted to 11.5 by the addition of aqueous 0.01 M NaOH and then stirring was continued for 3−4 h. The resultant product was washed thoroughly with deionized water. The sample was dried exclusively at room temperature before characterization. The organic matter was removed by calcining the sample at 600 °C for 24 h.

Characterization. The elemental composition of the resultant solid products was analyzed by chemical analysis. The synthesized sample was characterized by X-ray diffraction, thermogravimetric analysis, and spectroscopic analysis (e.g., IR, ESR, UV−vis, NMR, etc.). The morphology of the material was studied by transmission electron microscopy (TEM). The X-ray diffraction pattern of the sample was recorded on a Rigaku RAD-X system using monochromatized Cu Kα radiation (40 kV 20 mA, 0.02° step size, scan speed 1°/min) over the scan range 1.5−10°.

The diffuse reflectance UV−vis spectrum was measured with a 340 Hitachi spectrophotometer. Powder samples were loaded in a quartz cell and spectra were collected in the 200−850 nm wavelength range against a standard.

The FTIR spectrum in the framework region (1300−400 cm^{-1}) was recorded on a Perkin-Elmer model spectrum 1000 using a KBr pellet. About 1 mg of a finely powdered sample was mixed with 300 mg of dried KBr and then pressed.

Thermal analysis was performed by simultaneous TG-DTA measurements using a Rigaku Thermoflex TG-8101D unit. (About 10 mg of the sample was placed in a platinum pan and was heated at a heating rate of 10 °C/min.)

N_2 adsorption and desorption isotherms were obtained at 77 K with a micromeritics ASAP 2000 instrument. The sample was first outgassed at 300 °C for 24 h. The volume of adsorbed N_2 was normalized to standard temperature and pressure. The BET surface area was calculated by applying the BET equation. The pore size distribution (PSD) was calculated using the desorption branch of the N_2 adsorption/desorption isotherm and the Barrett−Joyner−Halenda (BJH) formula.

ESR spectra were recorded on a JEOL JES-FE3XG ESR spectrometer at room temperature and 77 K.

^{51}V and ^{29}Si NMR spectra were recorded at 11.75 T on a Varian INOVA 500 NMR spectrometer with a CPIMS probe. ^{29}Si MAS spectra were measured at 99.3 MHz using a SiN rotor at 3 kHz. ^{51}V spectra were acquired at 131.375 MHz with 5.0 μs recycle delays using SiN rotors 5 mm in diameter without spinning and with spinning at 3 kHz. The chemical shifts were given in ppm from external tetramethylsilane (TMS) and $VOCl_3$ for ^{29}Si and ^{51}V, respectively. All spectra were recorded at room temperature.

Results and Discussion

Analytical Data. The molar composition of the gel as described in the experimental part is 1:0.12:92.6 M/TEOS:$(C_{16}H_{33}N(CH_3)_3$ Br):H_2O. In the present method a minimum amount of template has been used to synthesize V−MCM-41 in comparison to the earlier reports[10,12] by our knowledge. According to Monnier et al.[13] this may be due to the charge density matching between the surfactant and inorganic species. From the analytical data it has been found that the Si/V ratio is comparable to those in the initial gel that is in contrast to other vanadium-containing zeolites. In contrast to Al−MCM-41 the structure is stable at a higher vanadium content even after calcination.

XRD. X-ray powder diffraction pattern of V−MCM-41 as synthesized and calcined is shown in Figure 1. The pattern consists of four Bragg peaks that can be indexed to different *hkl* reflections. These reflections verify the presence of hexagonal phases. The as-synthesized sample was free from crystalline V_2O_5. After calcination, to decompose surfactant, the XRD pattern of V−MCM-41 shows better resolution that may be due to some atomic rearrangement occurring inside the mesoporous material during the calcination and d_{100} distance was reduced. For vanadium-substituted MCM-41 an enlargement of the unit cell parameters both for as-synthesized and calcined materials was observed. The unit cell parameter with vanadium content is shown in Table 1. Although the precise structure of the vanadium-containing silicate matrix is unknown, the presence of similar distinct reflections with those of vanadium-free M41S in the XRD pattern suggests a long-range order in the hexagonal phase of both the as-synthesized and calcined samples. The better resolution of (110), (200), (210), and (300) peaks indicate that the particularly high crystallinity was achieved at room temperature. The resolution of the XRD pattern increases with increasing vanadium content. The XRD peak width of the calcined sample of Si/V = 20 was rather narrow, confirming the higher crystallinity of the material. Bulk and structural characterization [XRD,

(13) Monnier, A.; Schüth, F.; Huo, Q.; Kumar, D.; Margolese, D.; Maxwell, R. S.; Stucky, G. D.; Krishnamurthy, M.; Petroff, P.; Firouzi, A.; Janicke, M.; Chamelka, B. F. *Science* **1993**, *261*, 1299

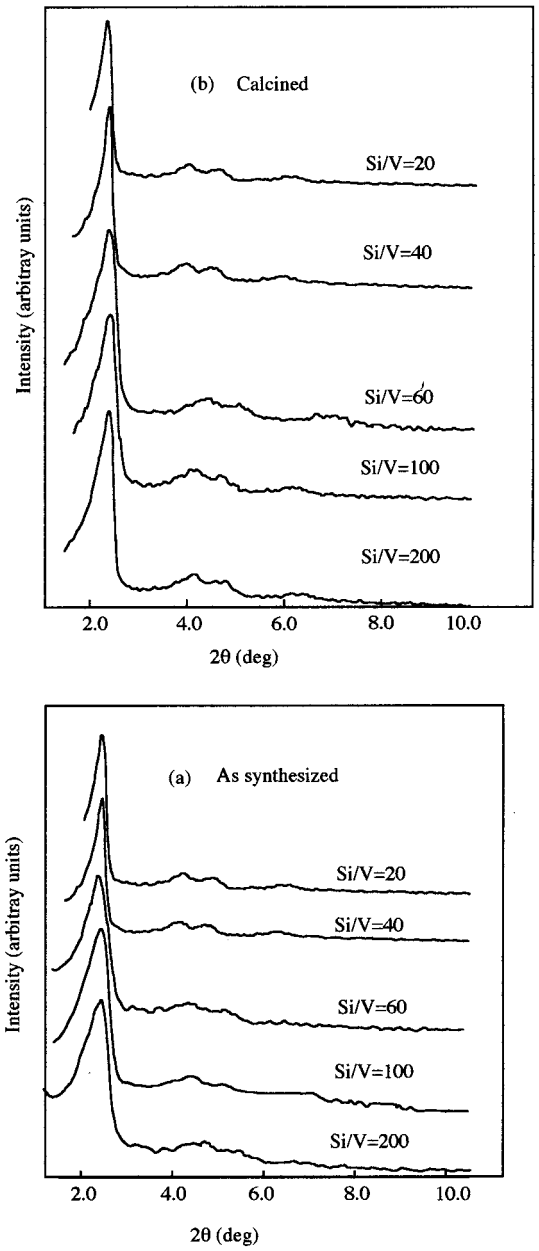

Figure 1. X-ray diffraction patterns of (a) as-synthesized and (b) calcined V−MCM-41 samples.

Table 1. Analytical Data[a]

sample	Si/V ratio	d_{100} (Å)	surface area ($m^2\ g^{-1}$)	pore volume (cm^3/g)	APD (Å)	a_o (Å)
1	200	36.7 (33.4)	960	0.76	26.4	42.4 (38.6)
2	100	37.7 (34.4)	1027	0.81	27.6	43.5 (39.7)
3	60	38.4 (35.8)	1079	0.94	28.9	44.3 (41.3)
4	40	39.7 (36.4)	1085	0.91	31.2	45.8 (42.0)
5	20	41.7 (37.0)	1095	0.96	34.0	48.1 (42.7)

[a] Figures in parentheses are for the calcined sample. APD = Average pore diameter; a_0 = the lattice parameter calculated from XRD data using the formula $a_0 = 2d_{100}/\sqrt{3}$.

BET(described latter)] data confirm the unit cell expansion with vanadium content. The presence of the (210) peak discards the possibility of wall thickness that is supported by the molecular dynamics calculation.[14] Hence, we can consider the probability of substitution of heteroatoms into the silicate structure. After calcination, the intensity of the XRD pattern increases significantly upon removal of the templated organic molecules.

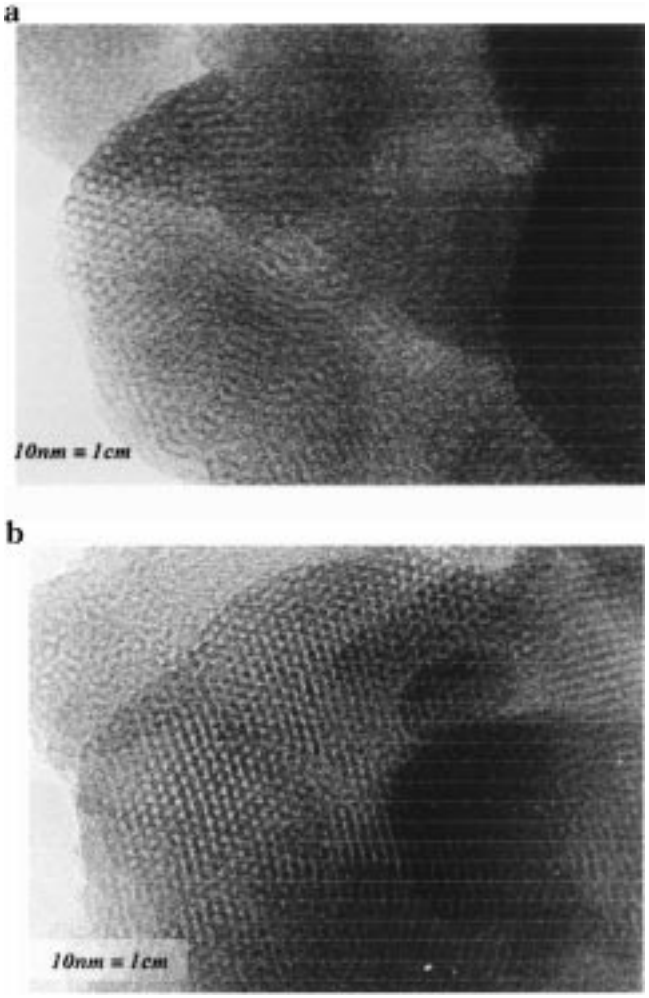

Figure 2. TEM photograph of (a) as-synthesized and (b) calcined V−MCM-41 (Si/V = 20) samples.

Transmission Electron Microscopy (TEM). The uniform mesopore structure of V−MCM-41 is evident in the transmission electron microscope lattice image (Si/V = 20) shown in Figure 2. TEM of the calcined sample shows the regular hexagonal array of uniform channels that is characteristic of MCM-41. The hexagonal structure with each pore surrounded by six neighbors is present in all samples. When viewed in the direction perpendicular to their axis, the pores were seen to be arranged in patches composed of regular rows. This is entirely consistent with the XRD results.

N_2 Adsorption−Desorption Isotherm. The N_2 adsorption−desorption isotherm and the Harvath−Kawazoe (HK) pore size distribution are presented in Figure 3. The isotherms were of type IV, typical of mesoporous solids. The inflection in the adsorption isotherm at $p/p_0 = 0.2-0.3$ indicates the mesopore filling. The p/p_0 coordinate of the inflection point depends on the pore size. The sharpness in this step suggests a uniform size pore system. Furthermore, the initial region can be extrapolated back to the origin, confirming the absence of any detectable micropore filling at low p/p_0. The isotherm contains an H3 hysteresis loop as defined by IUPAC[15] that is associated with solids with slit-shaped pores or plate-like particles.

(14) Feuston, B. P.; Higgins, J. B. *J. Phys. Chem.* **1994**, *98*, 4459.

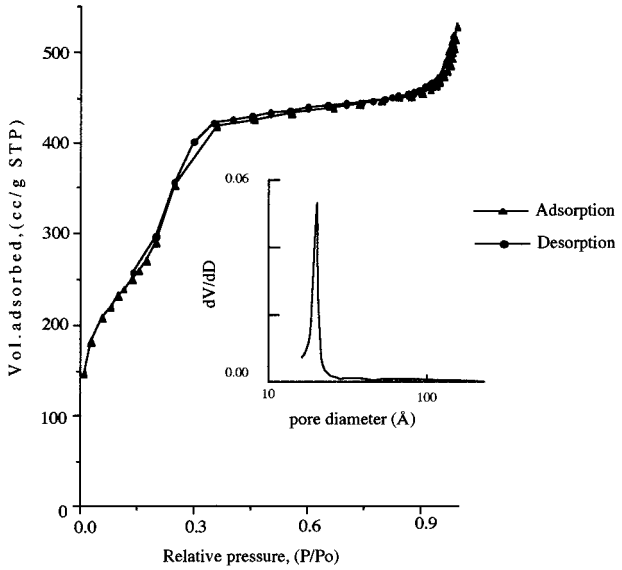

Figure 3. N_2 adsorption−desorption isotherm and pore size distribution of calcined sample (Si/V = 20).

The plot of the derivative of the pore volume per unit weight with respect to the pore diameter (d*V*/d*D*) is shown as an inset. The sharp pore size distribution confirms that those mesopores are exceptionally uniform. The BET surface area is close to 1079 $m^2\ g^{-1}$ and the average pore diameter is 28.9 Å.

Thermal Analysis. The thermal patterns are qualitatively very similar. The total weight loss occurs at three distinctive steps. Heating of the sample leads to the release of small amounts of water. The second weight loses starts at 150 °C and some steps were strongly exothermic. The exothermic step corresponds to the oxidative decomposition of the embedded template. About 60% of the template was decomposed in the second step. This may be assigned to the loosely bound template. The remaining template was removed only at a higher temperature. Hence, V−MCM-41 is a porous material and the thermal analysis curve has the same appearance as that of Si−MCM-41 as described in the literature.[7]

Framework FTIR. The FTIR spectra of the as-synthesized and calcined V−MCM-41 are shown in Figure 4. The spectra closely resemble those of the vanadium-free MCM-41. In the as-synthesized V−MCM-41, the asymmetric and symmetric stretching vibration bands appeared at about 1064 and 790 cm^{-1}, which was somewhat lower than those of vanadium-free MCM-41. In all samples a 960 cm^{-1} band was clearly visible. Such a band was assigned to Si−O stretching vibrations of $Si-O^- R^+$ groups as $R = H^+$ in the calcined state.[16] The strong intensity of this band in purely siliceous MCM-41 is due to the presence of a higher amount of silanol group in the calcined material. Although the origin and interpretation of this band are controversial,[17,18] an increasing intensity of this band with vanadium content may still be taken as proof of the incorporation of the metal ion in the structure. The change in the asymmetric stretching band position indicates the substitution of Si by V. The enhanced intensity of the 962 cm^{-1} band (with an increase in the vanadium content) in FTIR spectra is attributed to the V−O−Si linkage related to the nonextractable vanadium species in both the as-synthesized and calcined sample. Obviously, this criterion cannot be used to ascertain the incorporation of the metal ion; other techniques should be used to confirm this.

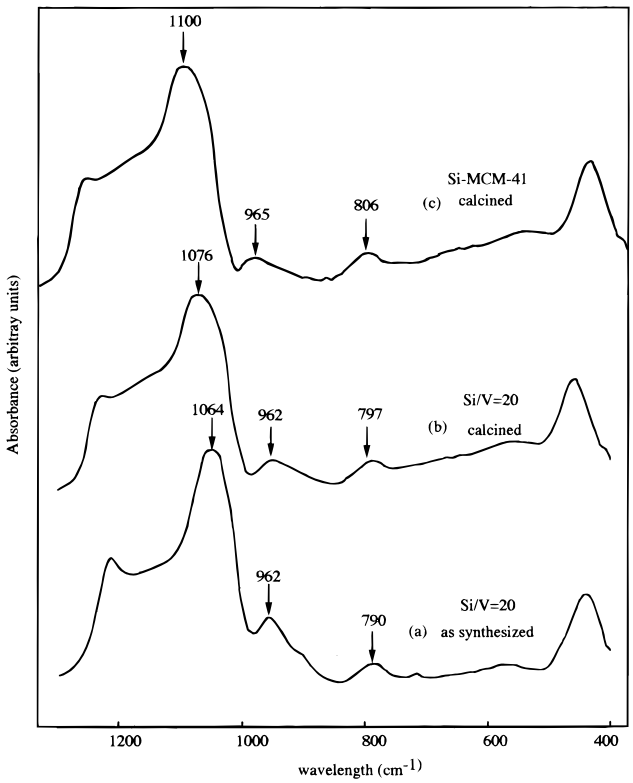

Figure 4. FTIR spectra of (a) as-synthesized V−MCM-41-(Si/V = 20), (b) calcined MCM-41 (Si/V = 20), and (c) calcined Si−MCM-41.

Diffuse Reflectance UV−Vis Spectrums. In general the UV−vis spectra of vanadium ions in the region examined associated with oxygen to vanadium electron transfer are characterized for V(V) ions. The lower energy charge-transfer (LCT) band for octahedral coordination is falling in the (20 000)−(30 000) cm^{-1} (333−500 nm) region. In tetrahedral vanadium compounds, in contrast, the LCT band is found at ∼30 000 cm^{-1} (333 nm) and the second charge-transfer (CT) transition band appears at ∼36 000 cm^{-1} (278 nm). The LCT transition for V(IV) falls at higher frequencies in the (35 000)−(40 000) cm^{-1} (286−250 nm) region, whereas the d−d transitions of VO^{2+} ions fall in the region of 13 000 cm^{-1} (769 nm) [$b_2(d_{xy}) \rightarrow e(d_{xy},d_{yz})$] and at or near 16 000 cm^{-1} (769 nm) [$b_2(d_{xy}) \rightarrow b_1(d_{x2-y2})$].[19] The d−d transition at higher frequencies [$b_2(d_{xy}) \rightarrow a_1(d_{x2})$] is generally masked by more intense charge-transfer transitions. The diffuse

(15) Sing, K. S. W.; Everett, D. H.; Houl, R. A. W.; Moscou, L.; Pierotti, R. A.; Rouquerol, J.; Siemieniewska, T. *Pure Appl. Chem.* **1985**, *57*, 603.

(16) Decottiguies, M.; Phalippou, J.; Zarzycki, J. *J. Mater. Sci.* **1978**, *13*, 2605.

(17) Corma, A.; Navarro, M. T.; Pérez-Pariente, J.; Sánchez, F. In *Zeolite and Related Microporous Materials: State of the Art 1994*; Weitkemp, J., Karge, H. G., Pfeifer, H., Hölderich, W., Eds.; Studies in Surface Science and Catalysis 84; Elsevier: Amsterdam, 1994; pp 69−75.

(18) López, A.; Tuilier, M. H.; Guth, J. L.; Delmotte, L.; Popa, J. M. *J. Solid State Chem.* **1993**, *102*, 480.

(19) Centi, G.; Perathoner, F.; Trifiro, A.; Aboukais, C. F.; Aissi, C. F.; Guelton, M. *J. Phys. Chem.* **1992**, *96*, 2617.

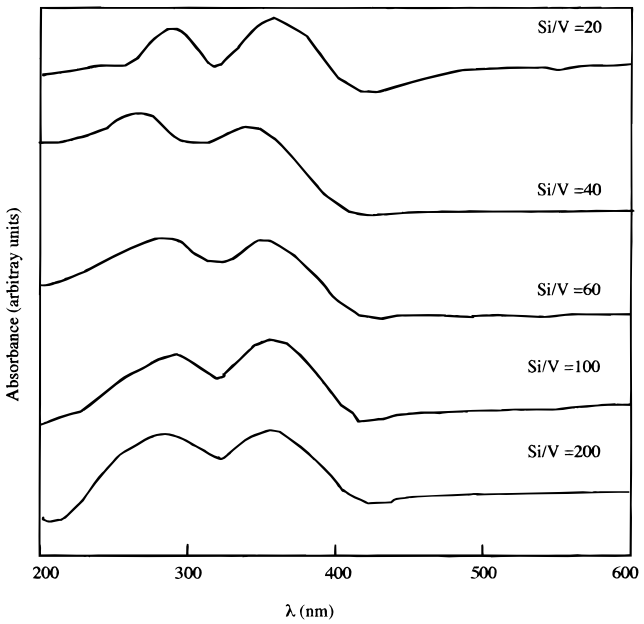

Figure 5. Diffuse reflectance UV−vis spectra of as-synthesized V−MCM-41 (a) Si/V = 200, (b) Si/V = 100, (c) Si/V = 60, (d) Si/V = 40, and (e) Si/V = 20.

reflectance UV−vis spectra of the as-synthesized and calcined samples were shown in Figure 5. In the case of the as-synthesized sample, it exhibits two intense absorption bands at 288 and 356 nm in the UV region. The doublet corresponds to the low-energy-charge transfer (LCT) bands assigned to O−V electron transfer (π)-$t_2 \rightarrow$ (d)e and (π)$t_1 \rightarrow$ (d)e, respectively, for tetrahedrally coordinated V^{5+} ions[20,21] which are colorless. Such a tetrahedral environment is typical for framework V^{5+} ions in zeolite. During synthesis V^{4+} ions become oxidized to V^{5+} ions. As there is no band in the visible region, samples may be purely white in color, but the ESR transition indicated the presence of a VO^{2+} ion. Since d−d transitions of VO^{2+} are weaker than those of the charge-transfer transition such absorption is apparently undetected by UV−vis. spectra. After calcination and hydration, the color of the sample changes from white to pale yellow. The spectrum still contains the doublet associated with tetrahedral V^{5+} ions. This indicates that those vanadium ions which are tetrahedrally coordinated directly after the synthesis remain stable in this coordination type. The absence of square pyramidal coordination in the freshly calcined form of the higher vanadium content sample again supports the stability of the tetrahedral coordination of vanadium in these samples. In calcined and hydrated (exposed to air for long time) sample the position of both bands remains the same, with broadening of these two bands which may be due to the additional coordination of the water molecule. Hence, according to the UV−vis spectra it can be concluded that two intense bands are detected at 288 and 356 nm described as tetrahedrally coordinated V^{5+} ions. After calcination, also the position of these bands remains the same which may further confirm the stability of the V^{5+} ion in the tetrahedral position. As

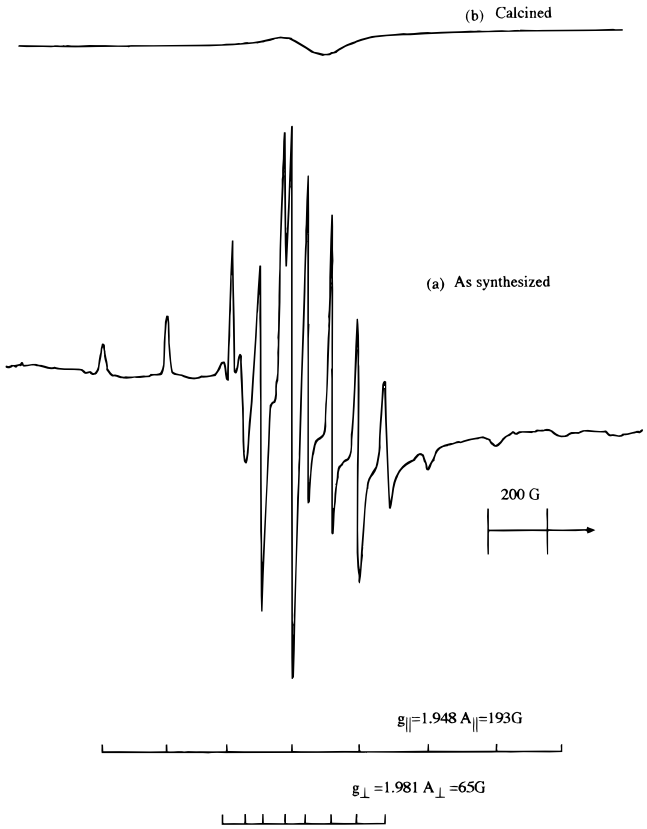

Figure 6. ESR spectra at 293 K of V−MCM-41 (Si/V = 20) (a) as-synthesized and (b) calcined.

there is no indication of other coordination states of the V^{5+}, ion the possibility of an octahedral arrangement was discarded.

Electron Spin Resonance (ESR). The ESR spectra (recorded at room temperature and 77 K) of all the as-synthesized vanadosilicates exhibit an axially symmetrical signal of tetravalent vanadium which originates from the d^1 electron interaction with nuclear spin $I_n = {}^7/_2$ of ^{51}V (natural abundance 99.8%). A representation of the ESR spectrum is shown in Figure 6. The ESR signal intensity of the as-synthesized material increases linearly with increasing vanadium content. The spectrum indicates only one vanadium site. The spin Hamiltonian parameters **A** tensor and **g** tensor are $\mathbf{g}_{||} = 1.948$, $\mathbf{A}_{||} = 191$ G, $\mathbf{g}_{\perp} = 1.991$, and $\mathbf{A}_{\perp} = 65$ G where **A** is the hyperfine coupling constant. The parameters of the spectra were independent of both the temperatures (298 or 77 K) and are close to those reported for V−ZSM-48.[22,23] A possible broad ESR signal, reflecting the presence of vanadium as any agglomerations of clusters, should range over the entire split that was not observed. No observation of spin−spin interactions among V^{4+} ions indicates that V^{4+} should be highly dispersed in the silicate matrix.

Upon calcination in static air at 600 °C spectra of vanadyl species disappeared completely, as did other reported vanadium-substituted molecular sieves.[20] This indicates that the VO^{2+} ion is oxidized to V^{5+}. No signal attributable to the V^{4+} ion could be detected in the calcined sample. The vacuum dehydrated the sealed

(20) Kornatowski, J.; Wichterlova, B.; Jirkovsky, J.; Loffler, E.; Pilz, W. *J. Chem. Soc., Faraday Trans.* **1996**, *92* (6), 1067.
(21) Schraml-Marth, M.; Wokaun, A.; Pohl, M.; Krauss, H.-L. *J. Chem. Soc., Faraday Trans.* **1991**, *87*, 2635.
(22) Kornatowski, J.; Sychev, M.; Goncharuk, V.; Baur, W. H. *Stud. Surf. Sci. Catal.* **1991**, *65*, 581.
(23) Rigutto, M.; van Bekkum, H. *Appl. Catal.* **1991**, *68*, L1.

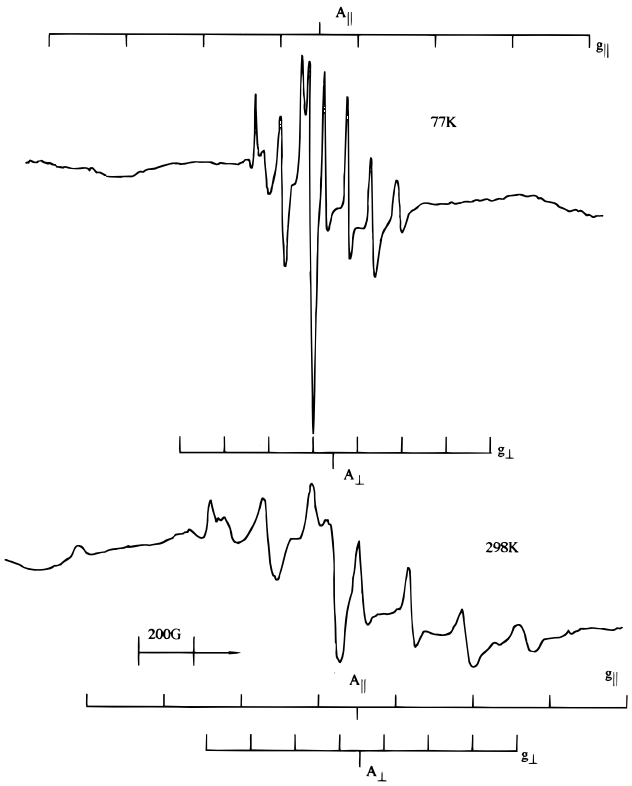

Figure 7. ESR spectra of calcined and reduced V−MCM-41 (Si/V = 20) at 293 K and 77 K.

sample, exhibiting eight lines of hyperfine spectra. To better characterize the nature of the vanadium species, the samples were reduced in hydrogen at 500 °C. Prior reduction of the calcined sample in H_2 recovered the original hyperfine structure of the spectra at 77 and 298 K (Figure 7). The ESR spectral features ($\mathbf{g}_{||} = 1.941$, $\mathbf{A}_{||} = 191$ G, $\mathbf{g}_{\perp} = 1.992$, $\mathbf{A}_{\perp} = 66$ G) with well-resolved hyperfine lines reflect unambiguously the presence of VO^{2+} in a square pyramidal coordination.[24−26] According to Davidson et al.,[27] it is very difficult to distinguish between an octahedral arrangement with square pyramidal one. This is since the sixth ligand is weakly bonded and only slightly modifies the unpaired electron distribution. In ESR spectra of both, geometries are characterized by $\mathbf{g}_{\perp} > \mathbf{g}_{||}$. The unpaired electron is assumed to be mainly living on the $3d_{xy}$ orbital of the metal. Hence, a factor $B = \Delta\mathbf{g}_{||}/\Delta\mathbf{g}_{\perp}$, indicator of tetragonal distortion, was introduced by Sharma et al.[28] An increase of *B* indicates a shortening of the V=O bond or a lengthening of the distance to the oxygen ligand in the basal plane. The *B*-value for the sample obtained by our method indicates a square pyramidal symmetry for the V^{4+} ion in the as-synthesized state as well as in the reduced state.

^{51}V Magic Angle Spinning NMR. The solid-state NMR spectrum of the ^{51}V isotope (spin 7/2) possesses a nuclear electric quadrupolar moment. The nuclear electric quadrupolar moment is affected by the interaction with electrostatic field gradients, created by asymmetric electrostatic environments. In a less asymmetric surrounding, the static NMR line shape is dominated by chemical shift anisotropy related to the three principle components of the nuclear magnetic shielding

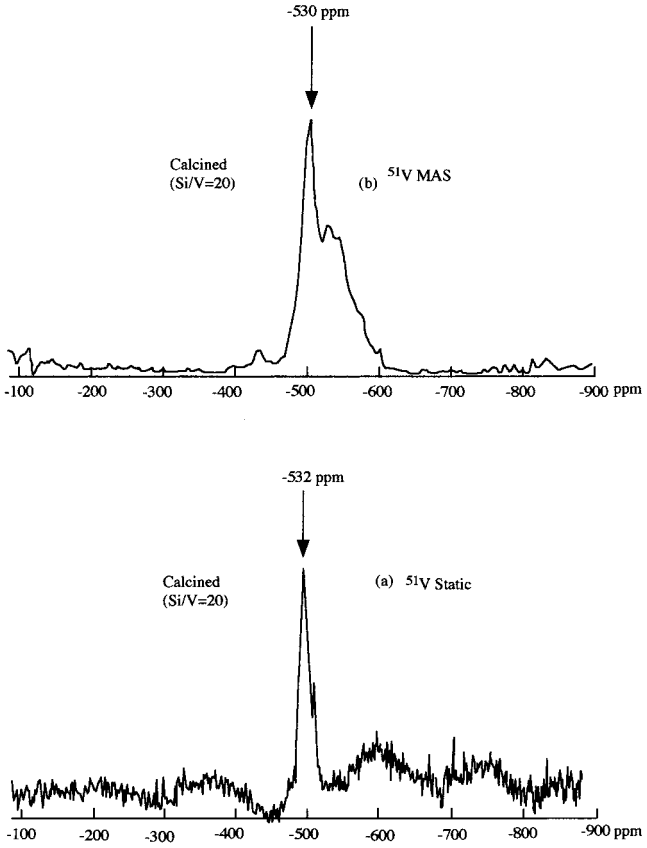

Figure 8. ^{51}V NMR spectra (a) static and (b) MAS of calcined V−MCM-41 (Si/V = 20).

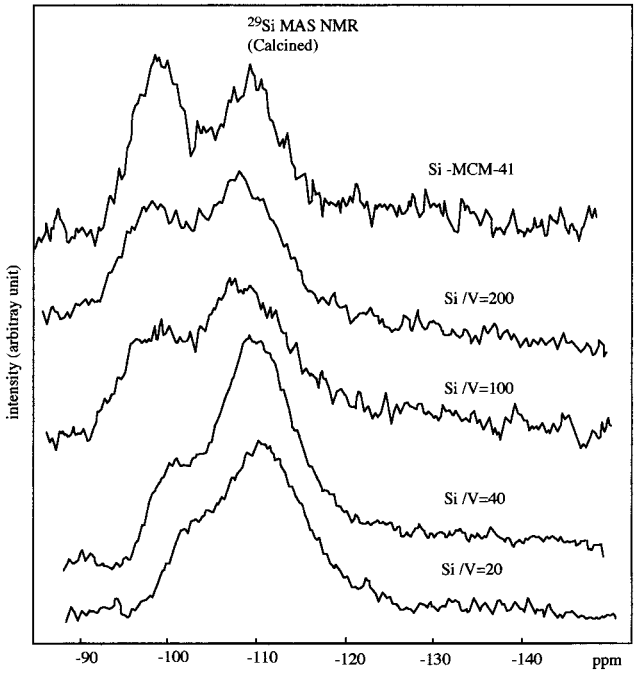

Figure 9. ^{29}Si MAS NMR spectra of V−MCM-41 compared to that of Si−MCM-41.

(24) Martini, G.; Ottaviani, F.; Seravalli, G. L. *J. Phys. Chem.* **1975**, *79*, 1716.
(25) Kornatowski, J.; Sychev, M.; Kuzenkov, S.; Strandova, K.; Pilz, W.; Kassner, D.; Pieper, G.; Baur, W. H. *J. Chem. Soc., Faraday Trans.* **1995**, *91*, 2217.
(26) Kornatowski, J.; Wichterlova, B.; Rozwadowski, M.; Baur, W. H. *Stud. Surf. Sci. Catal.* **1994**, *84*, 117.
(27) Davidson, A.; Che, M. *J. Phys. Chem.* **1992**, *96*, 9909.
(28) Sharma, V. K.; Wokaun, A.; Baiker, A. *J. Phys. Chem.* **1986**, *90*, 2715.

Table 2. Oxidation of Toluene[a]

			products (mol %)				
sample	conv (%)	H_2O_2 selectivity[a] (%)	benzaldehyde	*o*-cresol	*p*-cresol	benzyl alcohol	others
V−MCM-41	20.8	66.2	62.0	20.0	14.0	2.0	2.0
V−Al-beta[b]	14.0	64.8	56.0	21.0	17.0	4.0	2.0
VS-2[c]	11.7	49.5	52.2	19.7	17.1	7.7	3.7

[a] Reaction conditions: 100 mg of catalyst; toluene: H_2O_2 mole ratio = 3:1; toluene: catalyst = 10:1; temperature = 80 °C; solvent = acetonitrile. H_2O_2 utilized in the formation of benzaldehyde, benzyl alcohol, and cresols. [b] As described in the reference *J. Chem. Soc., Chem. Commun.* **1995**, 207. [c] As described in the reference *J. Catal.* **1993**, *141*, 595.

tensor. An independent piece of information on the strength of the quadrupolar interaction can be obtained from the field dependent MAS NMR. The resonance position is affected by a second-order quadrupolar shift $\delta^{(2)}$ such that $\delta_{exp} = \delta^{(2)} + \delta_{iso}$. For a spin of 7/2 nucleus this second-order quadrupolar shift amounts to $\delta^{(2)}$ (ppm) $= -2551\nu_0^{-2}\,(e^2qQ/h)^2(1 + \eta^2/3)$ where ν_0 is the nuclear larmor precision frequency in cps and e^2qQ/h and η are the principle component and the asymmetric parameter, respectively, of the nuclear electric quadrupolar interaction.[25]

Therefore, in all cases the NMR line shape gives useful information to differentiate between the various local coordination environments of vanadium sites better than that obtained from analysis of the isotropic shift alone. The as-synthesized sample does not give any NMR active signal, which could be due to the absence of any diamagnetic vanadium species. Figure 7a shows ^{51}V NMR spectra of the calcined hydrated sample recorded at the magic angle spinning condition and static condition. Since the ^{51}V isotope has a moderately large nuclear electric quadrupolar moment, wide line spectra can be complex because of to the simultaneous line-broadening effects arising from second-order quadrupolar and chemical shift anisotropy interactions. Eckert and Wachs[29] showed that line shapes usually are dominated by chemical shift anisotropy rather than by quadrupolar effects. In this case, the approximate shift value of the tensor that corresponds to singularities and the shoulder on the experimental spectrum are identical to three principle shift tensor components δ_{11}, δ_{22}, and δ_{33}. The signal at $\delta = -531.8$ ppm (relative to $VOCl_3$) is a strong indication of tetrahedral vanadium (V)[30] (Figure 8). It is well-known from the literature that the solid-state ^{51}V NMR line shape of the vanadium compound is determined by the symmetry of oxygen environments. Sparingly, the more inequivalance between bond length and angles in a VO_n unit, the more anisotropy observed in the spectra. So, compounds of vanadium with near equivalence of all V−O bonds can be characterized by spectra with an isotropic line. According to the literature, it is possible to differentiate between different types of four coordinated vanadates by ^{51}V NMR spectra such as $Q^{(1)}$, $Q^{(2)}$, and $Q^{(0)}$ species where the numbers in the parentheses indicate the number of bridging oxygen atoms that connect two vanadium polyhedra. For $Q^{(2)}$ species the anisotropy value is up to 250 ppm and a highly asymmetric tensor. For $Q^{(1)}$ species asymmetry is similar to that of $Q^{(2)}$, but in the case of $Q^{(0)}$ a low value of anisotropy associated with a relatively symmetric tensor was observed.[28] Vanadium species in calcined V−MCM-41 can be placed in the last series because of its low value of anisotropy and asymmetry values. Hence, it is in good agreement with the presence of vanadium species (V^{5+}) in a tetrahedral position in the framework. It is important to note that the ^{51}V NMR spectra give no indication of the presence of V_2O_5 in any of our samples. The presence of V_2O_5 can be estimated from the appearance of an NMR line near −300 ppm. In this region a perpendicular component of an axially anisotropic spectrum of V_2O_5 can be detected at very low concentrations.

^{29}Si MAS NMR. ^{29}Si MAS NMR spectra (Figure 9) of the as-synthesized sample consist of some broad peaks. On the basis of the chemical shifts the peak at −109 ppm has to be assigned to the $Si(OSi)_4$ (Q_4) sites and the line at −102 ppm is attributed to the $Si(OSi)_3OH$ (Q_3) site. The observed spectrum was relatively poor in comparison to that of Si−MCM-41. There was a progressive reduction in the intensity of Q_3 (because of the large number of silanol groups in Si−MCM-41 Q_3 intensity is always higher) sites with increasing vanadium content. It strongly supports metal-promoted cross-linking of the mesoporous wall.

Catalytic Results. It has been shown above that the different physicochemical techniques indicate that in the V−MCM-41 samples the vanadium is in the framework positions. Therefore, it could be active for carrying out catalytic oxidation of hydrocarbons using peroxides as oxidants whereas the pure silica analogue was completely inactive. Here, we have carried out the oxidation of toluene and the hydroxylation of benzene and compared it with the result as described by a previous author in the case of a vanadium-containing zeolite. The oxidation of toluene and the hydroxylation of benzene were carried out batchwise in a flask. The reaction conditions for the hydroxylation of benzene were as follows: 25 mg of catalyst, 100 mmol of benzene, 30 mmol of H_2O_2 (30%), 343 K reaction temperature, and 24 h of reaction time. The solution of the hydroxylation product was colorless. Only phenol was formed by this hydroxylation reaction and conversion was 97.4%; H_2O_2 selectivity was 79%. The oxidation of toluene was carried out at 353 K for 24 h using 100 mg of catalyst, 10 mL of solvent (acetonitrile), 1 g of reactant, and a 3 mole ratio of reactant to H_2O_2. The products were analyzed by gas chromatography (GC 17A) using a capillary column. The results are given in Table 2. The oxidation of toluene produced benzaldehyde and *o*- and *p*-cresols as the major products whereas in the case of the hydroxylation of benzene the major product was phenol (not included in the table). The possibility of the leaching out of vanadium into solution from the solid in the presence of aqueous H_2O_2 was also considered. To evaluate this problem, we used a method employed by Neumann and Levin-Elad.[31] In this method the

(29) Eckert, H.; Wachs, I. E. *J. Phys. Chem.* **1989**, *93*, 6796.
(30) Tanev, P. T.; Pinnavaia, T. J. *Science* **1995**, *267*, 865.

catalyst was treated with H_2O_2 at reaction temperature in the presence of a different solvent (for example, water, ethanol, acetonitrile, etc.); after that, the catalyst was separated by filtration. To check the activity, an organic substrate was added to the solution but no catalytic activity was detected. Hence, the contribution of the dissolved vanadium ions to the rate of reaction is considered to be negligible. However, to obtain better results, the above oxidation reaction was carried out in the presence of terbutylhydroperoxide (TBHP) as the oxidant. In that case, also, the same activity was observed. Hence, catalytic activity is related to the nonextractable V^{5+} ion only.

Conclusion

The present study demonstrates that mesoporous materials containing highly dispersed vanadium and having a hexagonal structure can be synthesized at room temperature. Several techniques were employed to characterize vanadium centers in this material obtained from a very simple process. The state of vanadium in the as-synthesized and calcined sample has been implied from consideration of the experimental data. Different spectroscopic techniques confirm the presence of vanadium in the 5+ state. The tetrahedral environment of V−MCM-41 was obtained, without any hydrothermal treatment, containing only one type of VO^{2+} ion that is ESR-active. This class of V−MCM-41 materials is potentially of interest because of their high catalytic activity in oxidation reactions.

Acknowledgment. M.C. gratefully acknowledges the financial support from the Science and Technology Agency of Japan.

CM981152K

(31) Neumann, R.; Levin-Elad, M.; *Appl. Catal.* **1995**, *122*, 85.